where i is either TE or TM and

$$Z_{TE} = \frac{j\omega\mu_o}{\gamma_{mn}}, \qquad Z_{TM} = \frac{\gamma_{mn}}{j\omega\epsilon} \tag{8}$$

The tangential fields are sufficient to define the normalized Floquet volts.gewaves [9] at a plane z as they represent power travelling in the $\pm z$ direction. Note that in defining the TE and TM folds, such as shown in (5) and (6), they have been normalized to obtain a symmetric scattering matrix for reciprocal structures,

$$\int\int_{\substack{\text{unit}\\ \text{cell}}} \vec{\mathbf{e}}_i^{\pm} \times \vec{\mathbf{h}}_i^{\pm} \cdot (\pm\hat{\mathbf{z}})\, dS = 1, \quad i = TE \text{ or } TM \tag{9}$$

Since the normalizing direction, $\pm\hat{\mathbf{z}}$, is dependent on whether the waves are forward or backward travelling. Therefore the sign of either $\vec{\mathbf{e}}_{TE}$ or $\vec{\mathbf{h}}_{TE}$ must change dependent on the direction of propagation. As mentioned previously, it is convenient to choose the sign of the electric field components to remain the same, except for the necessary change on γ_{mn},

$$\vec{\mathbf{e}}_i^{+} = \vec{\mathbf{e}}_i^{-} \quad \text{and} \quad \vec{\mathbf{h}}_i^{+} = -\vec{\mathbf{h}}_i^{-} \text{ for } z = \text{O, i} = TE \text{ or } TM \tag{lo}$$

to guarantee that reflection from a pcc plate will give a reflection coefficient of -1

The total tangential electric field at a reference plane $z = z'$ is then weighted by the appropriate coefficients of the normalized Floquet harmonics,

$$\vec{\mathbf{E}}_i(m,n) = C_i^{+}(m,n)\, \vec{\mathbf{e}}_i^{+}(m,n) + C_i^{-}(m,n)\, \vec{\mathbf{e}}_i^{-}(m,n) \quad i = TE \text{ or } TM \tag{11}$$

where $C_{TE}^{\pm}(m,n)\, \vec{\mathbf{e}}_{TE}^{\pm}(m,n)$ is analogous to the forward travelling volt age On a transmission line. Likewise the magnetic field will correspond to the forward travelling current, which is related to the electric field via *(7). So* that the scattering parameters can be defined at port i due to an incident Floquet harmonic at port j,

$$S_{ij} = \frac{C_i^{\pm}(m,n)\, \vec{\mathbf{e}}_i^{\pm}(m,n)}{C_j^{\mp}(m,n)\, \vec{\mathbf{e}}_j^{\mp}(m,n)} = \frac{C_i^{\pm}(m,n) e^{\pm\gamma_{mn}z'}}{C_j^{\mp}(m,n) e^{\mp\gamma_{mn}z'}} \tag{12}$$

where tile reference plane is located at $x = y =$ O and $z = z'$.

C. Power Waves at the Device Under Test (D.U. 7'.)

It is now necessary to define the scattering parameters at the device ports due to incident Floquet harmonics. For the planar geometry as shown in Fig. 1, the device port locations ate not terminated in

transmission lines with known characteristic impedance. Therefore it is necessary to choose generalized power waves as described by Kurokawa [12].

$$a_i = \frac{V_i + Z_i I_i}{2\sqrt{|\mathrm{Re} Z_i|}} \tag{13}$$

$$b_i = \frac{V_i - Z_i I_i}{2\sqrt{|\mathrm{Re} Z_i|}} \tag{14}$$

By convenience, the normalizing impedance Z_i at the ith port is chosen to be the input impedance. Thus the scattering parameters as given by (12) are determined with the device ports matched, $V_i = -Z_i I_i$, so that $a_i = 0$.

The scattering parameters between the ith incident Floquet harmonics and kth device ports are then computed via

$$S_{ki} = -I_k \sqrt{|\mathrm{Re} Z_k|} \tag{15}$$

And by reciprocity, the scattering parameters due to excitation at the device ports are found by using the symmetry of the resulting scattering matrix. The input reflection coefficient at the kth device location, S_{kk} is then computed by

$$S_{kk} = \frac{Z_k - Z_k^*}{Z_k + Z_k^*} \tag{16}$$

Thus equations (12), (15), and (16) define the generalized scattering matrix for the periodic array. Note that when the supporting superstrate and substrates materials are lossless, the computed generalized scattering matrix satisfies the usual conditions related to power conservation. In the next section waveguide simulation approach and measured results will be presented

III. Waveguide Simulation

Fig. 3 shows the one port dipole unit cell to be simulated in a waveguide simulator. The substrate is supported by Rogers RT/duroid 5880, $\epsilon_r = 2.2$, that is 0.32 cm thick. To support two orthogonal modes for two port device measurements, the unit cell was placed in square waveguide. The dimensions of one edge of the square unit cell is 4.74 cm, and the dipole has a length of 4.0 cm and width of 0.44 cm. The dipole is loaded with a chip resistor of length 0.1 cm, width 0.5 cm, and height of 0.04 cm.

Fig. 4 shows a simplified diagram of the one port device in the waveguide. In this simplified diagram, the generalized scattering matrix computed by the procedure outlined above results in a three port scattering matrix relating the field quantities at ports 1 and 3, to the power wave representation at the device port. Upon calibration at the waveguide ports, the computed generalized scattering matrix then forms the embedding network to which the chip resistor is attached. Since the scattering matrix for this embedding network is known, the scattering parameters of the chip resistor load can be determined from measurements at waveguide ports 1 and 2.

In the more general case which uses a square unit cell the measurement of the two orthogonal TE modes, TE_{01} and TE_{10}, in the square waveguide are required. For measurement of these two orthogonal modes, orthomode junctions become part of the embedding network as shown in Fig. 5. Therefore the generalized scattering matrix for the unit cell, S^{num}, is represented by a 5 port generalized scattering matrix for a one port device, and a 6 port generalized scattering matrix for a two port device. The composite scattering matrix resulting from the combination of S^{num} with the measured scattering parameters of the orthomodes formed a 4 port embedding network. Measurement of the resulting 4 port scattering matrix then allowed for extraction of S^{dut}.

A. Test Setup Characterization

Addition of the orthomode junctions into the measurement setup requires measurement of the S parameters of these 4 port devices. Determination of the S parameters of the orthomodes is complicated by the need to place standards at the square waveguide port that match one of the TE modes, while reflecting the orthogonal mode with known magnitude and phase. This was accomplished by using a stepped transition in one dimension from 4.74 cm to 3.27 cm, and then from 3.27 cm to rectangular waveguide of 2.21 cm by 4.74 cm which only supports one dominant TE mode. A mode matching solution was used to calculate the magnitude and phase of the stepped transition so that it could be used as a standard in determination of the S parameters of the orthomode junctions.

In order for the relatively narrow band stepped transitions to exhibit greater than 20 dB return loss, and to avoid introduction of the higher order TE_{11} and TM_{11} modes, it was necessary to limit the measurement range from 4.0 GHz to 4.4 GHz. Note that the addition of the orthomodes creates a source of uncalibrated

error in t he measurement system, which is calibrated in rectangular waveguide. Assessment of errors due to the presence of the orthomodes was dorm by connecting; two "identical" orthomodes so that their square waveguide ports arc together. The external ports presented t hen allow for a four port measurement in rcct angular waveguide. 'J 'bus the perfect "thru" junction between tile two orthomodes can be de-embedded. This measurement indicated a maximum of 8% error in magnit udc of one propagat ing mode, and 3% error in the magnitude of the orthogonal square wave.guide mode with phase error less than 2.2 degrees for both modes.

The usc of square waveguide for simulation of a periodic array requires the solution of the periodic array problem for the two Floquet modes composing the TE_{01} mode. These plane waves arc incident at the angle θ which varies from 46 to 52 degrees over the frequency range of measurement. This large angle of incidence results in additional reflection of the $m = -1$ Floquet harmonic, which must be properly combined with the two original exciting modes when forming S^{num}. In order to satisfy the boundary conditions of the square waveguide, a rot at ion of ϕ =- 90 degrees then computes the paramet ers for t he $TE_{10\ \text{mode}}$. Thus a 10 port representation of S^{num} using Floquet modes is reduced to a 6 port scattering matrix for waveguide simulation.

B. Results for a One Port D. U. T.

Fig. 6 snows the results of de-embedding the S parameters of the unit cell shown in Fig. 3 when the load is replaced hy a conducting patch. The de-embedded S parameter shown is normalized to the antenna input impedance. The superstrate layer for this unit cell consists an air layer of thickness 1 cm. The inclusion of the air superstrate layer allows the generalized scattering matrix for the array to be properly referenced to the interface of the support fixture for the unit cell, and the face of the orthomode junction. The support fixture used consisted of a square waveguide section of length 1.32 cm in which t he unit cell was press fitted. This allowed for removal and replacement of the device under test.

Fig. 7 shows the de-embedded S parameter for the unit cell shown in Fig. 3 when it is loaded with a 51 Ω chip resistor. The theoretical curve is computed by using the computed input impedance, Z_{in}, which is the normalizing impedance. The frequency dependence of these curves is due to the slight variation in the

input impedance which varies from (164.8 - j 8.2) Ω to (178.8 + j 6.1) Ω from 4.0 to 4.4 GHz. The maximum error in the measured magnitude of the device S parameter is 8.6%.

The load impedance magnitude and phase for the one port device can be calculated sinew the normalizing impedance, the input impedance at the device port Z_{in}, is known.

$$Z_{in} = \frac{S^{dut} Z_{in} - Z_{in}}{1 - S^{dut}} \tag{17}$$

'J 'he nonlinear nature of this conversion may increase or decrease the error in the measured S parameter S^{dut}, but puts the results in a more readable form. Fig. 8 shows the measured load impedance magnitude and phase as computed from (17). The measured load magnitude is in error by approximately 8.4%. As expected the relative error when represented by (17) was minimal when the loading chip resistor was more closely matched to the input impedance presented at the device. Although it was not done here, incorporation of error correction terms into the measurement system would alleviate these problems.

Before moving to results for two port devices it is noted that measured transmitted and reflected parameters of the loaded unit cell, such as those depicted by S_{21} and in S_{12} in Fig. 4, where also measured and compared to theoretical results. These 4 port parameters were, in general, of similar accuracy to the load de-embedding results presented. This provided another method of verifying a composite S^{num} formed from the combination of the Generalized scatter'illg parameters for the periodic array and the S parameters of the device.

C. Results for a Two Port D. U. T.

Fig. 9 shows the two port unit cell used for waveguide simulation. The substrate and individual dipole dimensions arc the same as the single dipole shown in Fig. 3. By separating orthogonal chip resistors by a thin layer of polyimide, each individual dipole was loaded independently with no connection to the other device. In this configuration equation (17) can be used to de-embed the load impedance values from the measured data. Fig. 10 shows the measured results when two 120 Ω chip resistors arc used. The average error on the vertical loaded port, port 5, is 4.4% while the average error on the horizontal port is 15.8%. This is more error than expected duc to a worst case linear summation of the two polarizations of the orthomodes, 11%. The maximum phase angle measured was 24 degrees.

D. Results for a Differential Pair HEMT Two Port D. U. T.

Since it is difficult to measure the differential pairs often used in grid amplifiers [3-5], waveguide simulation of a single unit cell provides a means of measuring, these parameters. The unit cell configuration shown in Fig. 9 was used to measure a differential pair HEMT wire bonded in tile con figuration shown in Fig. 1. Upon measurement of the 4 port scattering matrix at the external rectangular waveguide ports of the two orthomode junctions, the 2 port S parameters of the differential HEMT pair were extracted for different bias levels.

The differential pair is in common source configurat ion with DC ground applied to t he sources through a 50 Ω resistor. '1 'he gates are self-biasing. Fig. 11 shows the de-embedded two port S parameters of the differential pair HEMT. The devices are biased with a drain bias of 5 V and 8 mA. To put the generalized scattering parameters in a more standard form, Fig. 11 shows scattering, parameters normalized to 50 ohms. Note the large mis-match of the devices to both input ant] output ports, as represented by S11 and S22, for this normalizing impedance. Even with the mis-matches on input and output the necessary conditions for stability

$$|S11| < 1, \quad |S22| < 1 \tag{18}$$

are satisfied. Fig. 12 shows the scattering parameters normalized to 50 ohms when the drain bias becomes o v.

Fig. 13 shows the magnitude of the generalized scattering parameters as computed, where the normalizing impedances are the input impedances at the ports. This corresponds to the act ual device loading presented by the grid during the waveguide measurement. The result is a more desirable match to the device at higher frequencies as shown. And as the input match improves, the transducer power gain, S21, increases until a the maximum of 0.8 dB is reached at 4.4 GHz.

IV. Conclusions

A generalized scattering matrix for modeling of grid amplifier and oscillator arrays has been developed and verified experimentally. The method incorporates generalized scattering matrix representation for the periodic array, where Floquet harmonics represent ports of the array. These additional ports are combined

with power wave representations of at the device ports which a re in the plane of t he array. The advantages of t his approach are that magnetic and electric wall assumptions arc not needed. Also the Floquet mode representation allows for the combination of polarizers and other periodic structures commonly used in quasi-optical setups by cascading of scattering matrices [9], while allowing for non-normal incidence and inclusion of coupling effects. A single unit cell was measured in a waveguide simulator for verification of the approach. Results for loaded dipoles with one port and two port devices were presented. Also measured scattering parameters of a single unit cell of a grid amplifier using a differential pair 11 EMT were presented.

ACKNOWLEDGEMENT

The authors thank Raul Perez for his measurement assistance, and Gilbert Chinn for analyzing the stepped transitions needed to measure the S parameters of the orthomode junctions.

References

[1] Z. B. Popović, R. M. Weikle II, M. Kim, and D. B. Rutledge "A 100 MESFET planar grid oscillator," *IEEE Trans. Microwave Theory and Tech.*, vol. 39, no. 2, pp. 193-200, Feb. 1991.

[2] R. M. Weikle II, M. Kim, J. B. Hacker, M. P. De Lisio, and D. B. Rutledge "Planar MESFET grid oscillators using gate feed back," *IEEE Trans. Microwave Theory and Tech.*, vol. 40, no. 11, pp. 1997-2003, Nov. 1992.

[3] R. M. Weikle II, M. Kim, J. B. Hacker, M. P. De Lisio, Z. B. Popović, and D. B. Rutledge "Transistor oscillator and amplifier grids," *Proc. IEEE*, vol. 80, pp. 1800-1809, Nov. 1992.

[4] M. Kim, J. J. Rosenberg, R. Peter Smith, R. M. Weikle, II, J. B. Hacker, M. P. DeLisio, and D. B. Rutledge, "A grid amplifier," *IEEE Microwave and Guided Wave Letters*, vol. 1, no. 11, pp. *322-324, Nov.* 1991.

[5] M. Kim, E. A. Sovero, J. B. Hacker, M. P. De Lisio, J. C. Chiao, S. J. Li, D. R. Gagnon, J. J. Rosenberg, and D. B. Rutledge "A 100-element HBT grid amplifier," *IEEE T* Pens. *Microwave Theory and Tech.*, vol. 41, no. 10, pp. 1762-1771, Oct. 1993.

[6] S. C. Bundy and Z. B. Popović, "A generalized analysis for grid oscillator design," *IEEE Trans. Microwave Theory and Tech.*, vol. 42, no. 12, pp. 24. S6-2491 , Dec. 1994.

[7] S. C. Bundy and Z. B. Popović, "Analysis of cascaded quasi-optical grids," *IEEE MTT-S Symp. Dig.*, vol. 2, pp. 601-604, May 1995.

[8] M. Guglielmi and A. A. Oliner, "Multimode network description of a planar periodic metal-stril) grating at a dielectric interface - part I: rigorous network formulations, " *IEEE Trans. Microwave Theory and Tech.*, vol. 37, no. 3, pp. 534-541 March 1989.

[9] P. A. Cwik and R. Mittra, "The cascade connection of planar periodic surfaces and lossy dielectric layers to form an arbitrary periodic screen ," *IEEE Trans. on Antennas and Propagat.*, w)]. 35, no. 12, pp. 1397-1405, I) Cc. 1987.

[10] R. C. Hall, R. Mittra, and K. M. Mitzner, "Analysis of multilayered periodic structures using generalized scattering matrix theory" *IEEE Trans. on Antennas and Propagat.*, vol. 36, no. 4, pp. 511-517, April 1988.

[11] N. K. Das and I). M. Pozar, "Multiport scattering analysis of genera] multilayered printed antennas fed by multiple feed ports: part I - theory," *IEEE Trans. on Antennas and Propagat.*, vol. 40, no. 5, pp. 469-481, May 1992.

[12] P. C. Sharma and K. C. Gupta, "A generalized method for de-embedding of multiport networks," *IEEE Trans. on Instrumentation and Measurement,* vol. I M-30, pp. 305-307, Dec. 1981.

[13] K. M. Mitzner, "Effective boundary conditions for reflection and transmission by and absorbing shell of arbitrary shape," *IEEE Trans. on Antennas and Propagat.*, vol. AP-16, no. 6, pp. 706-712, Nov. 1968.

[14] C.H. Tsao ant] R. Mittra, "Spectral-domain analysis of frequency selective surfaces comprised of periodic arrays of cross dipoles and Jerusalem crosses, " *IEEE Trans. on Antennas and Propagat.*, vol. AP-32, no. 5, pp. 478-486, May 1984.

[15] T. Itoh, "Spectral domain immitance approach for dispersion characteristics of generalized printed transmission lines," *IEEE Trans. Microwave Theory and Tech.*, vol. MTT-28, no. 7, pp. 733-736, July 1980.

[16] C. H. Chan and R. Mittra, "On the analysis of frequency selective surfaces using subdomain basis functions," *IEEE Trans. on Antennas and Propagat.*, vol. 38, no. 1, pp. 40-50, Jan. 1990.

[17] L. Epp, C. H. Chan, and R. Mittra, "The study of FSS surfaces with varying surface impedance and lumped elements " *Abstracts of the 1989 IEEE AP-S International Symposium*, San Jose, CA, vol. 2, pp. 1056-1059, June 1989.

[18] V. Galindo, N. Amitay, and C. P. Wu, *Theory and analysis of phased array antennas. New* York: Wiley-Interscience, 1972.

[19] K. Kurokawa, "Power waves and tile scattering matrix," *IEEE Trans. Microwave Theory and Tech.*, vol. MTT-13, pp. 194-202, March 1965.

[20] J. S. H. Schoenberg, S. C. Bundy, and Z. B. Popović, "Two-level power combining using a lens amplifier," *IEEE Trans. Microwave Theory and Tech., vol.* 42, no. 12, pp. 2480-248 5, Dec. 1994.

[21] R. A. York, P. Liao, and J. J. Lynch, "Oscillator array dynamics wit] ı broadband N-port coupling networks," *IEEE Trans. Microwave Theory and Tech.*, vol. *42, no. 11,* pp. 2040-2045, *Nov.* 1994.

[22] J. Fang and D. Xeu, "Numerical errors in the computation of impedances by FDTD method and ways to eliminate them," *IEEE* Microwave *and Guided Wave Letters*, vol. 5, no. 1, pp. 6-8, Jan. 199].

Figure Titles

Fig. 1. Overview showing distinction between the generalized scattering matrix of the grid, S^{num}, and the differential pair device under test. Note that input and output are separated by orthogonal polarizations at normal incidence.

Fig. 2. General form of generalized scattering matrix containing n+m Floquet modes in region 1 and region 2.

Fig. 3. Unit cell of one port device for waveguide simulation. The substrate is RT/duroid 5880 with ϵ_r = 2.2 and a thickness of 0.32 cm (0.125"). The port is terminated with a chip resistor of length 0.1 cm, width 0.05 cm and height of 0.04 cm.

Fig. 4. Waveguide method of one port S parameter de-embedding using a single unit cell. Note that S31, S21, ... are computed by numerical analysis.

Fig. 5. Waveguide method of two port S paramter de-embedding using a single unit cell and two orthomode junctions to verify S^{num} and measure S^{dut}.

Fig. 6. De-embedded S^{dut} parameters using the unit cell shown in Fig. 3 when the load is a conducting patch, (a) measured S11 magnitude and (b) measured S11 phase.

Fig. 7. De-embedded S^{dut} parameters using the unit cell shown in Fig. 3 when the load is a 51 ohm chip resistor, (a) measured S11 magnitude and (b) measured S11 phase.

Fig. 8. De-embedded load impedance of the unit cell shown in Fig. 3 when the load is a 120 ohm chip resistor, (a) measured load magnitude and (b) measured load phase.

Fig. 9. Unit cell of two port device for waveguide simulation. The substrate is RT/duroid 5880 with ϵ_r = 2.2 and a thickness of 0.32 cm (0.125"). The port is terminated with a differential pair HEMT designed and fabricated at JPL.

Fig. 10. De-embedded two port S^{out} load impedances of the unit cell shown in Fig. 9 when the loads are two 120 ohm chip resistors, (a) measured load magnitude and (b) measured load phase.

Fig. 11. Magnitude of de-embedded device S parameters, normalized to 50 ohms, when the unit ccl] shown in Fig. 9 is loaded with a differential pair HEMT biased at 5 V, 8.0 rnA.

Fig. 12. Magnitude of de-embedd device S parameters, normalized to 50 ohms, when the unit cell shown in Fig. 9 is loaded with a differential pair HEMT biased at O V.

Fig. 13. De-embedded device S parameters, normalized to input impedances, when the unit cell shown in Fig. 9 is loaded with a differential pair HEMT biased at 5 V, 8.0 mA.

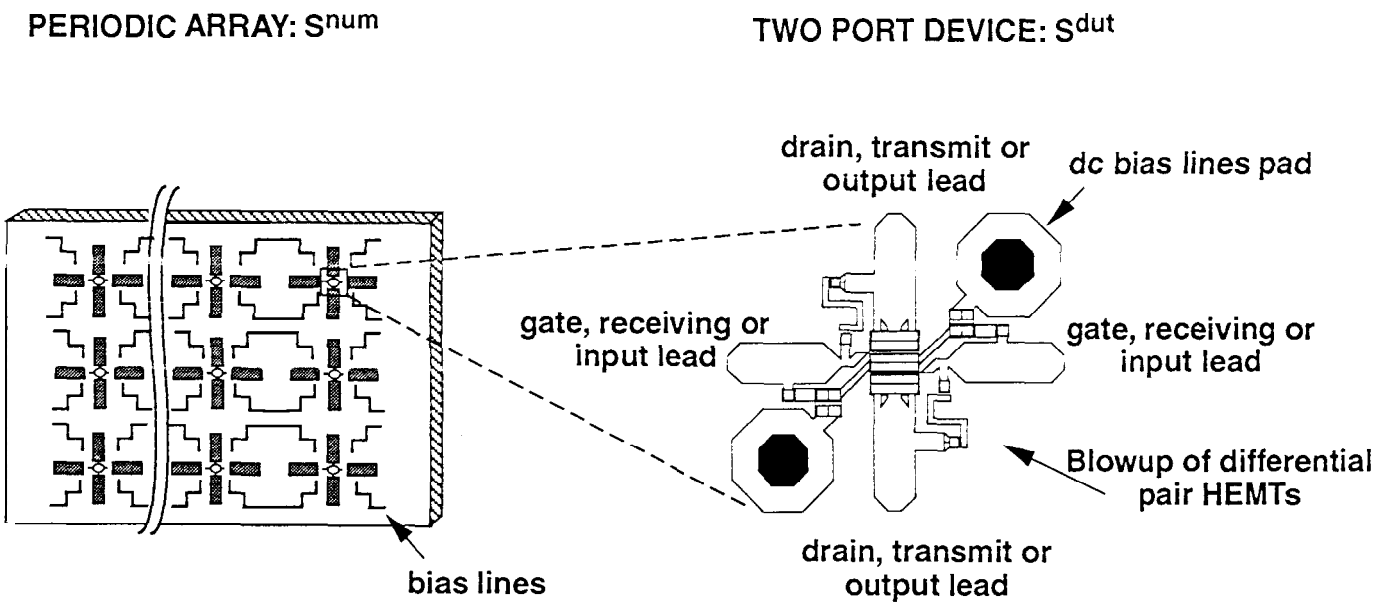

Fig. 1. Overview showing distinction between the generalized scattering matrix of the grid, S^{num}, and the differential pair device under test. Note that input and output are separated by orthogonal polarizations at normal incidence.

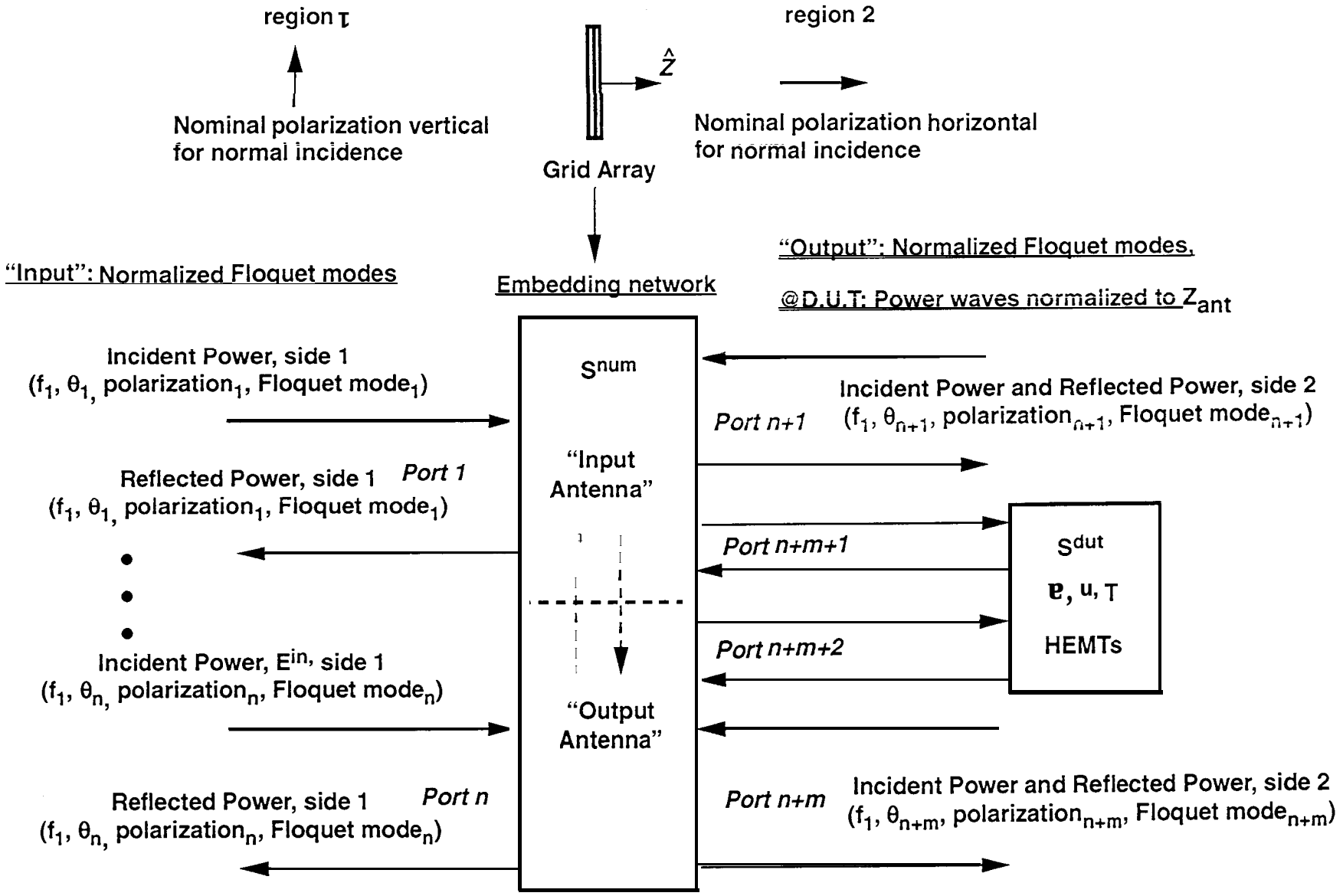

Fig. 2. General form of generalized scattering matrix containing n+m Floquet modes in region 1 and region 2.

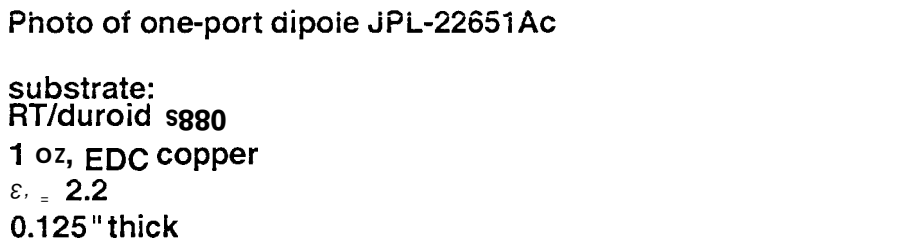

Fig. 3. Unit cell of one port device for waveguide simulation. The substrate is RT/duroid® 5880 with ε_r = 2.2 and a thickness of 0.32 cm (0.125"). The port is terminated with a chip resistor of length 0.1 cm, width 0.05 cm and height of 0.04 cm.

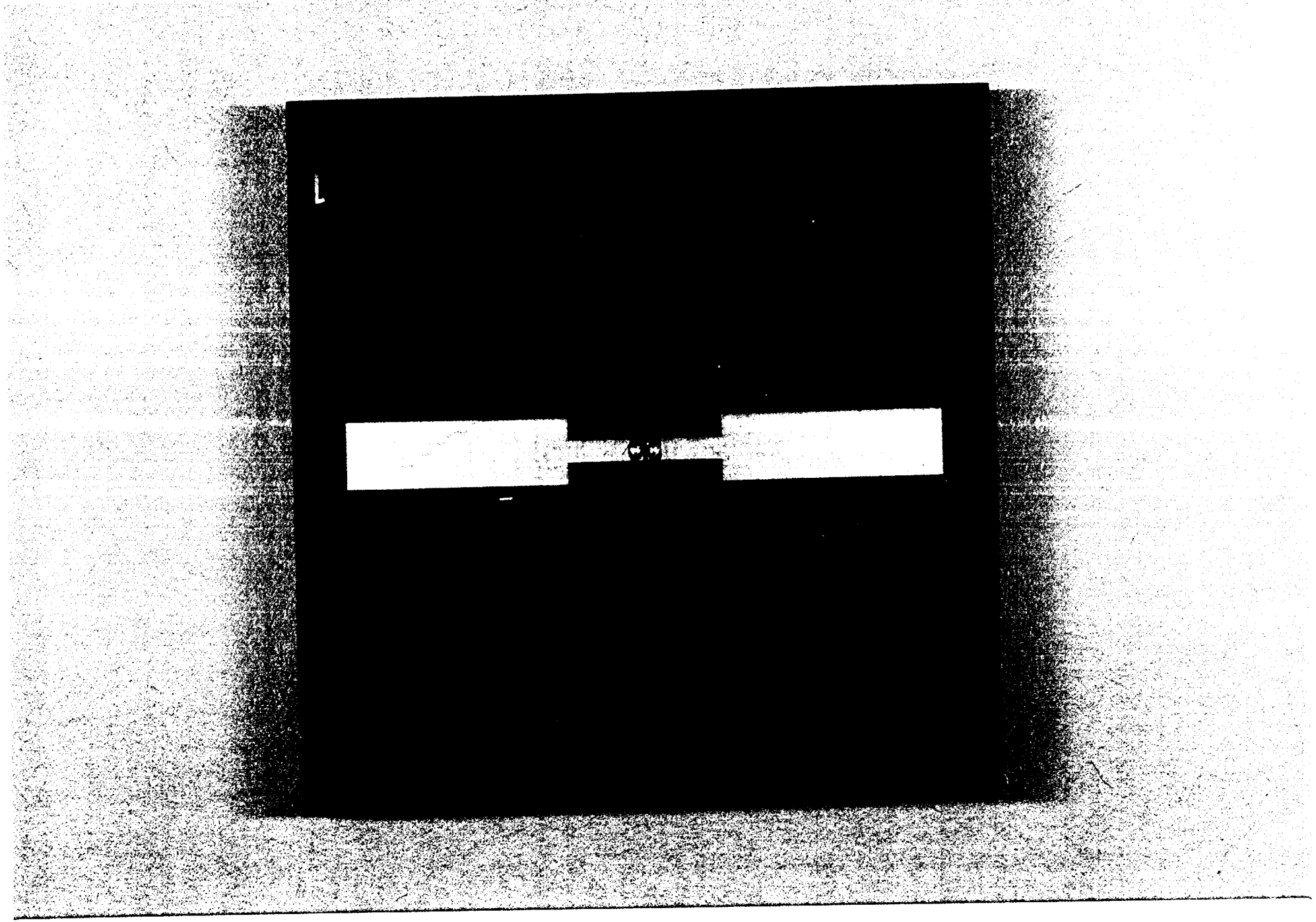

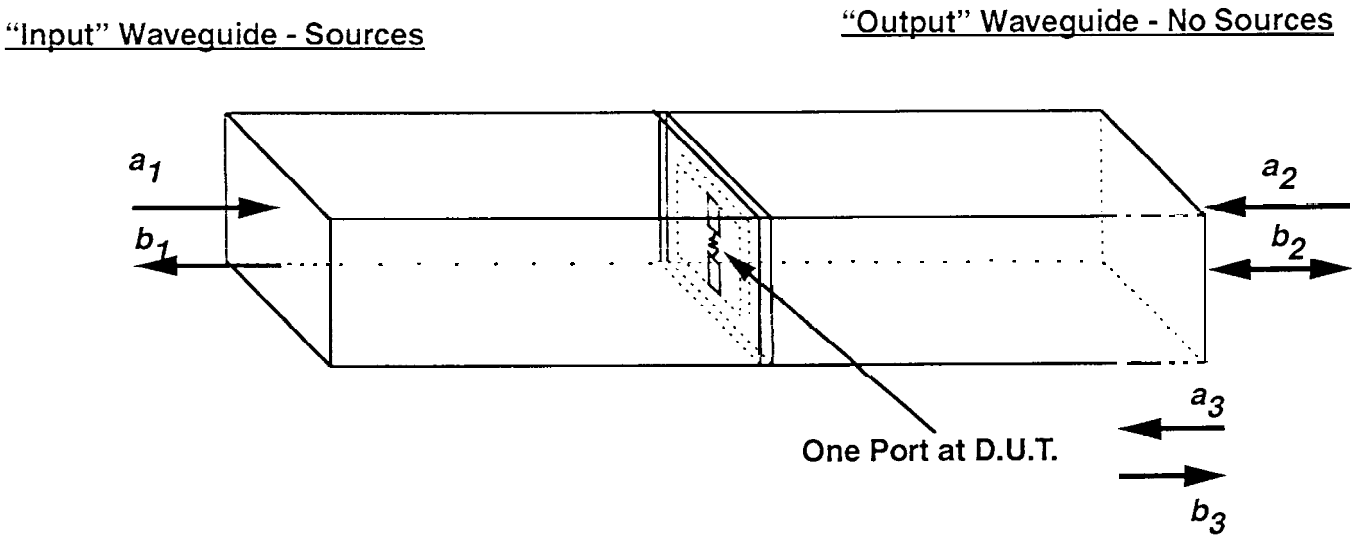

Fig. 4. Waveguide method of one port S parameter de-embedding using a single unit cell. Note that S31, S21, ... are computed by numerical analysis.

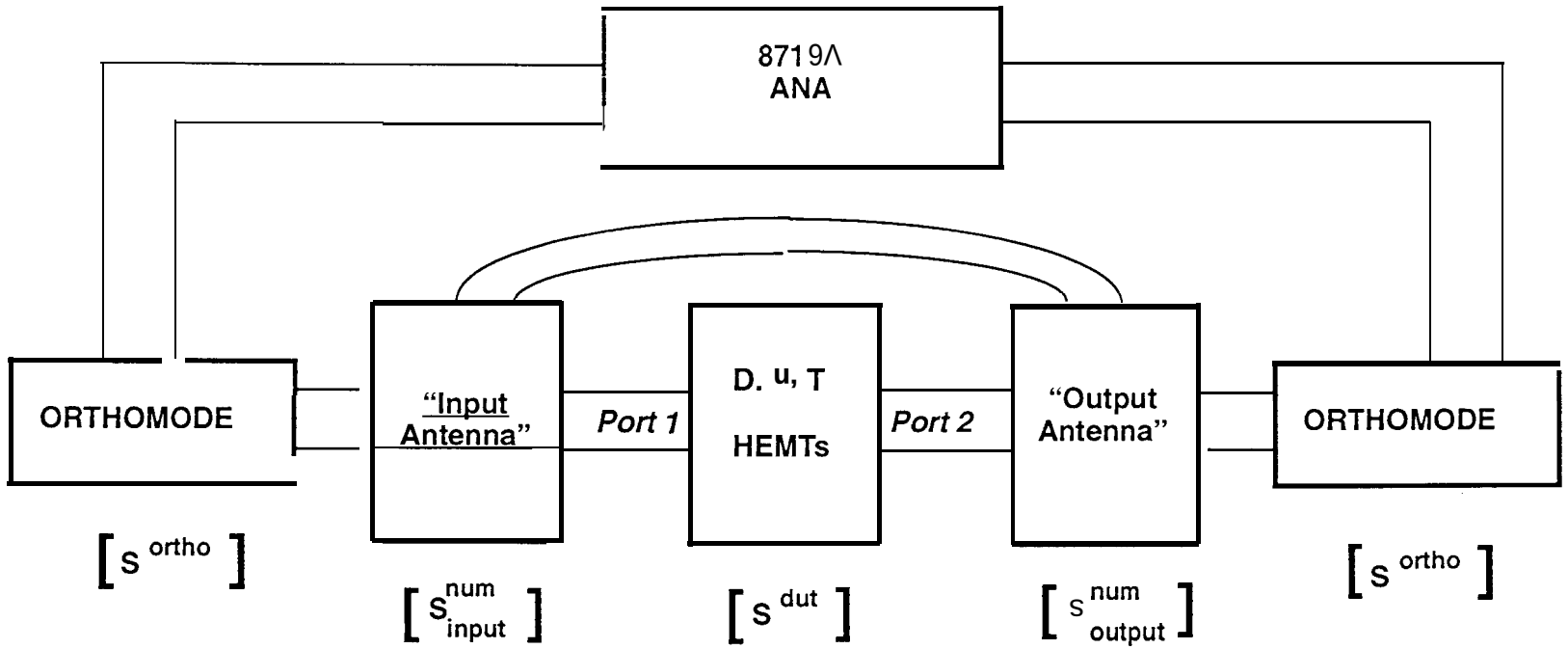

Fig. 5. Waveguide method of two port S parameter de-embedding using a single unit cell and two orthomode junctions to verify S^{num} and measure S^{dut}.

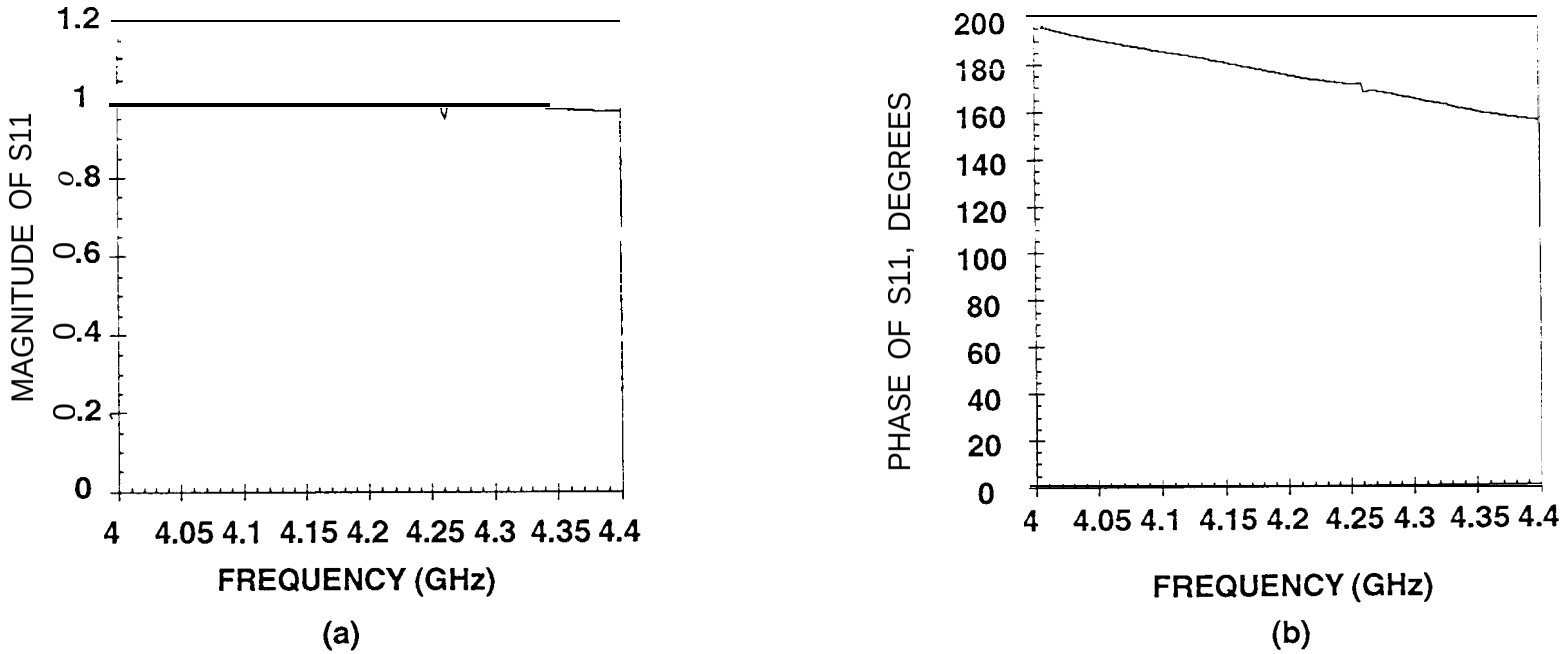

Fig. 6. De-embedded S^{dut} parameters using the unit cell shown in Fig. 3 when the load is a conducting patch, (a) measured S11 magnitude and (b) measured S11 phase

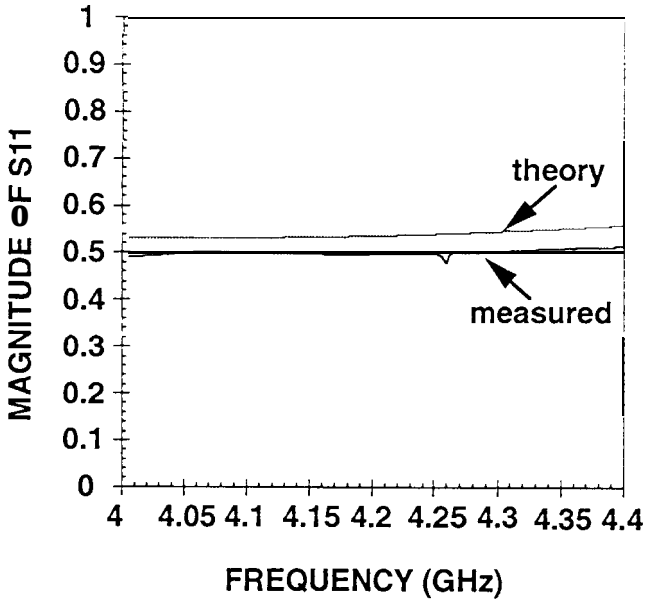

(a)

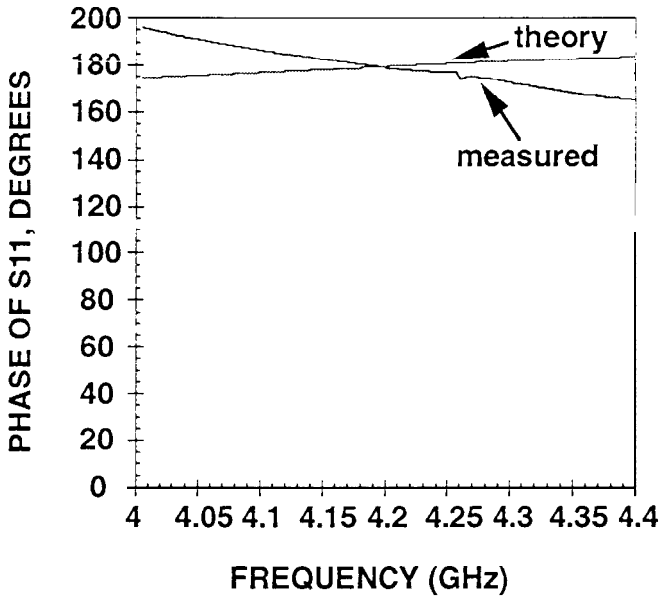

(b)

Fig. 7. De-embedded S^{dut} parameters using the unit cell shown in Fig. 3 when the load is a 51 ohm chip resistor, (a) measured S11 magnitude and (b) measured S11 phase

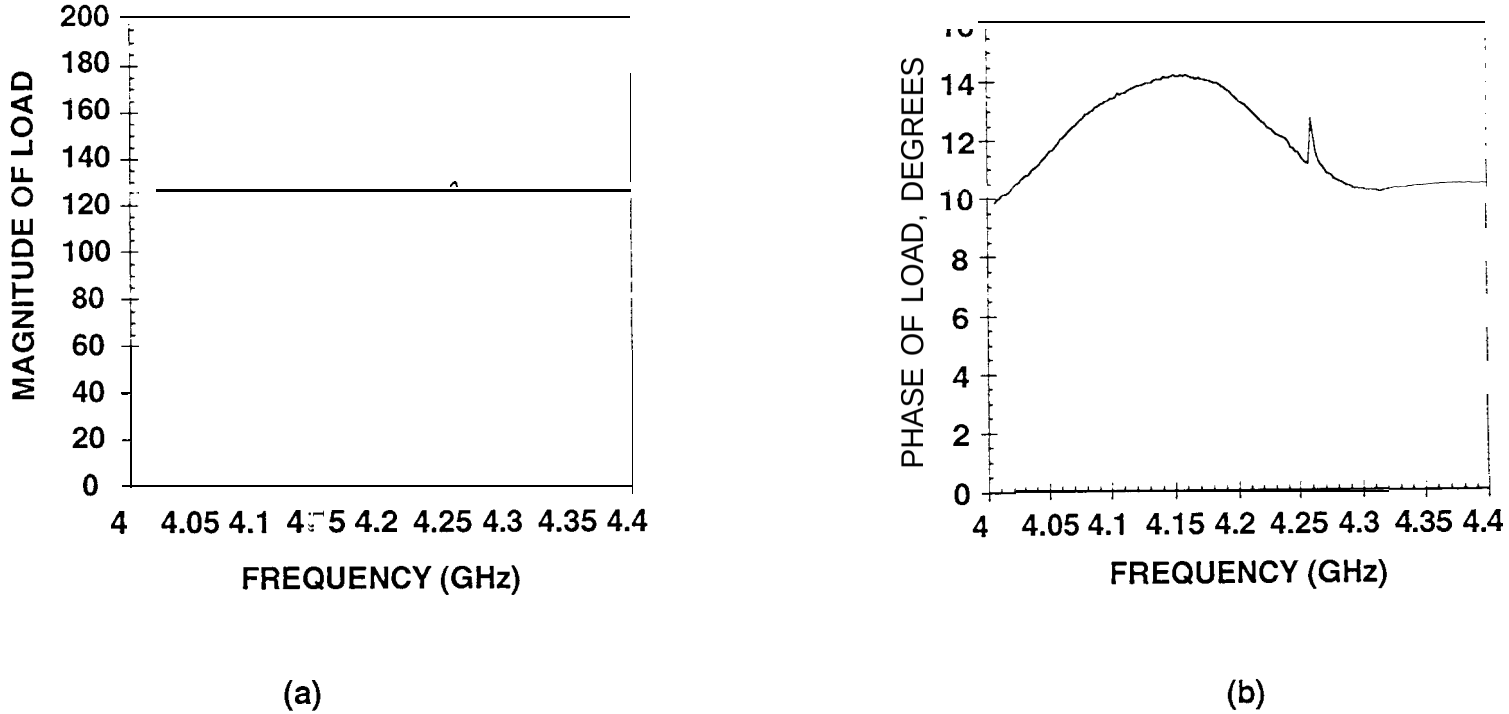

Fig. 8. De-embedded load impedance of the unit cell shown in Fig. 3 when the load is a 120 ohm chip resistor, (a) measured load magnitude and (b) measured load phase

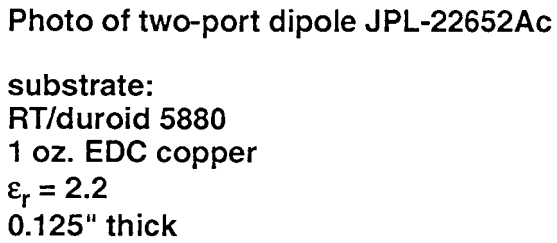

Fig. 9. Unit cell of two port device for waveguide simulation. The substrate is RT/duroid® 5880 with $\varepsilon_r = 2.2$ and a thickness of 0.32 cm (0.125"). The port is terminated with a differential pair HEMT designed and fabricated at JPL.

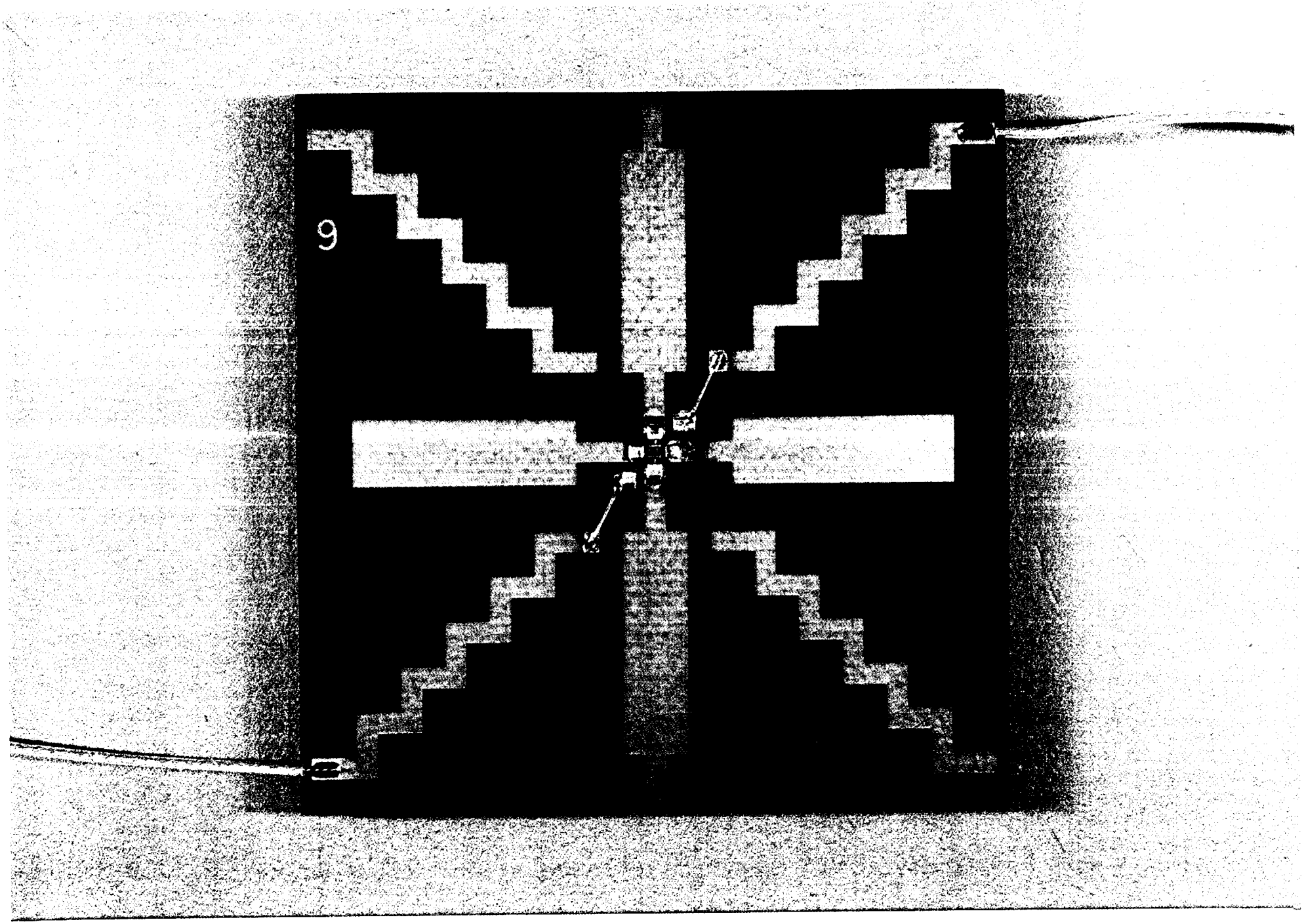
9

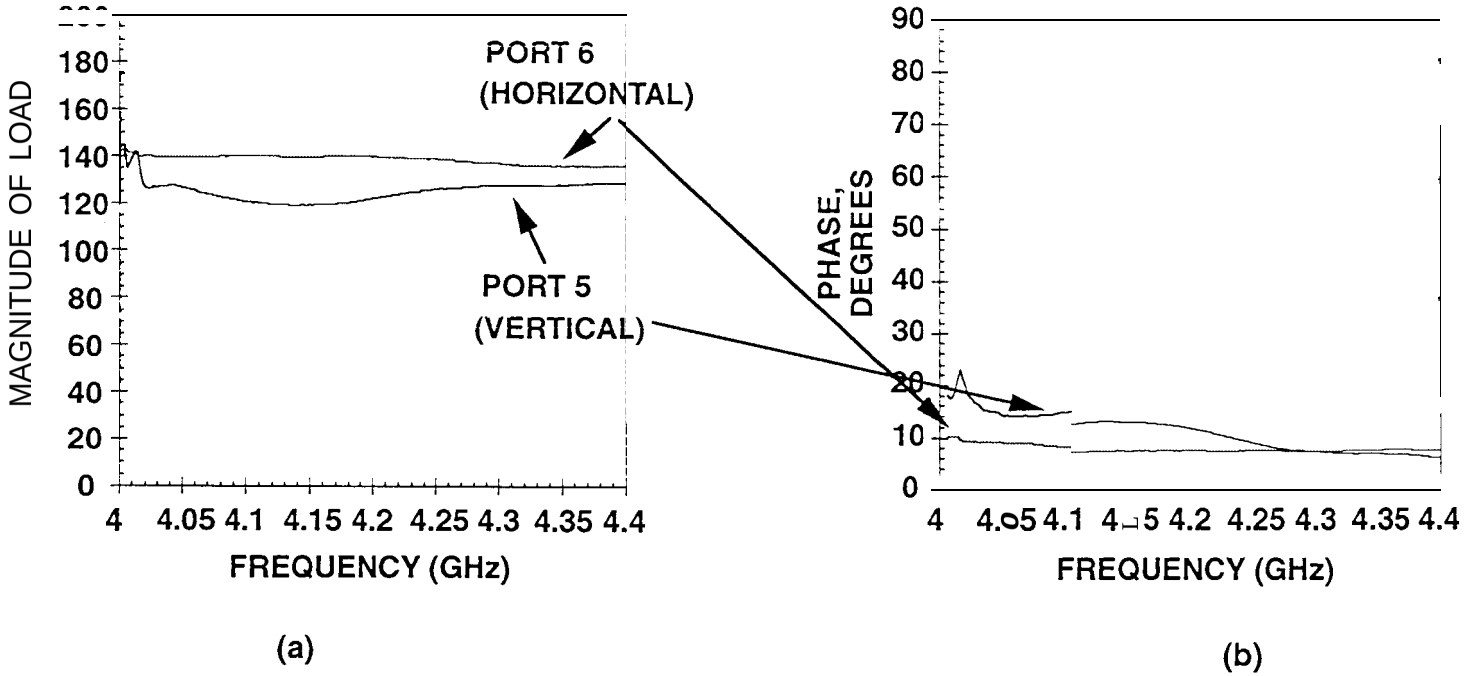

Fig. 10. De-embedded two port S^{dut}: load impedances of the unit cell shown in Fig. 9 when the loads are two 120 ohm chip resistors, (a) measured load magnitude and (b) measured load phase

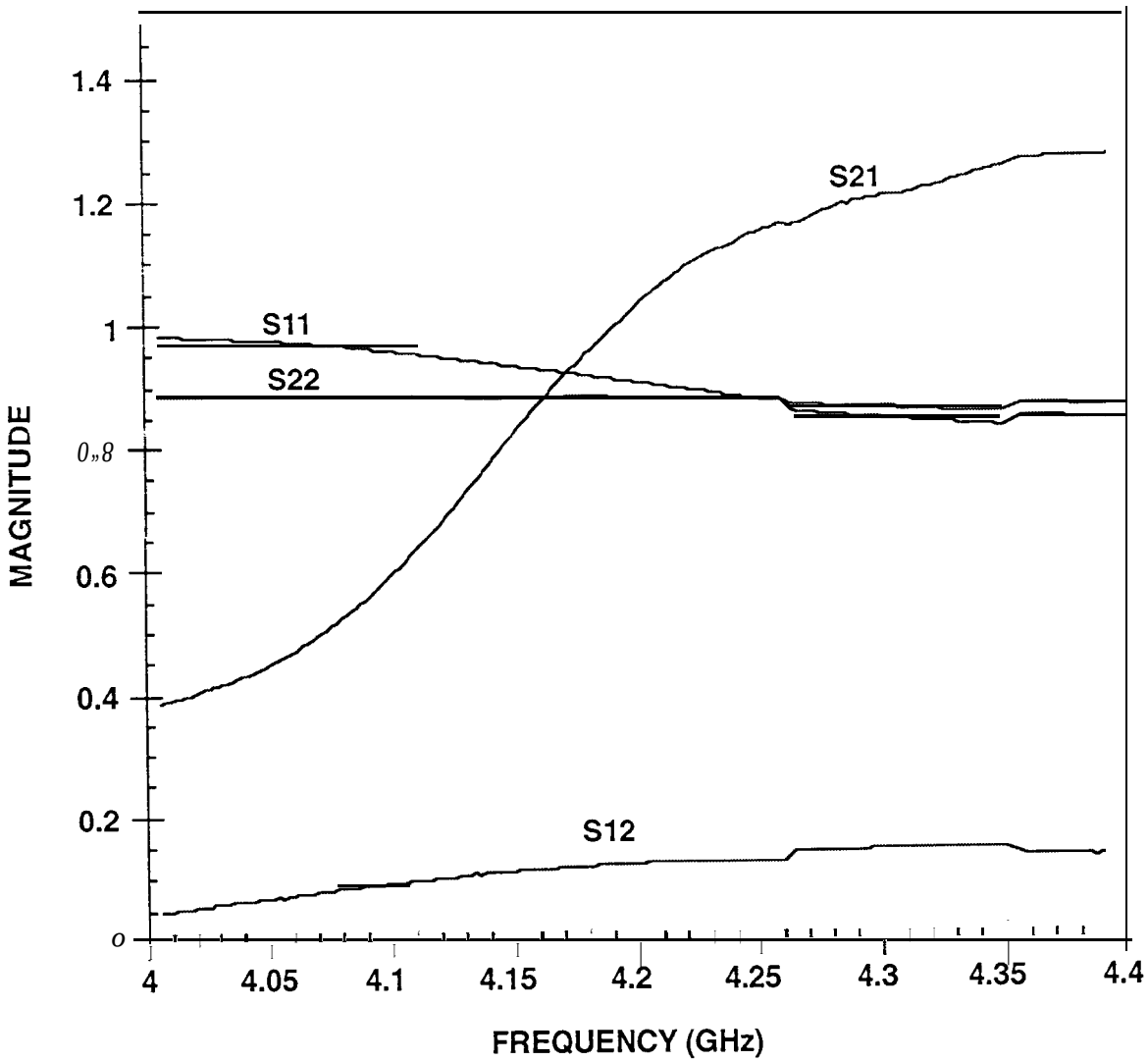

Fig. 11. Magnitude of de-embedded device S parameters, normalized to 50 ohms, when the unit cell shown in Fig. 9 is loaded with a differential pair HEMT biased at 5V, 8.0 mA.

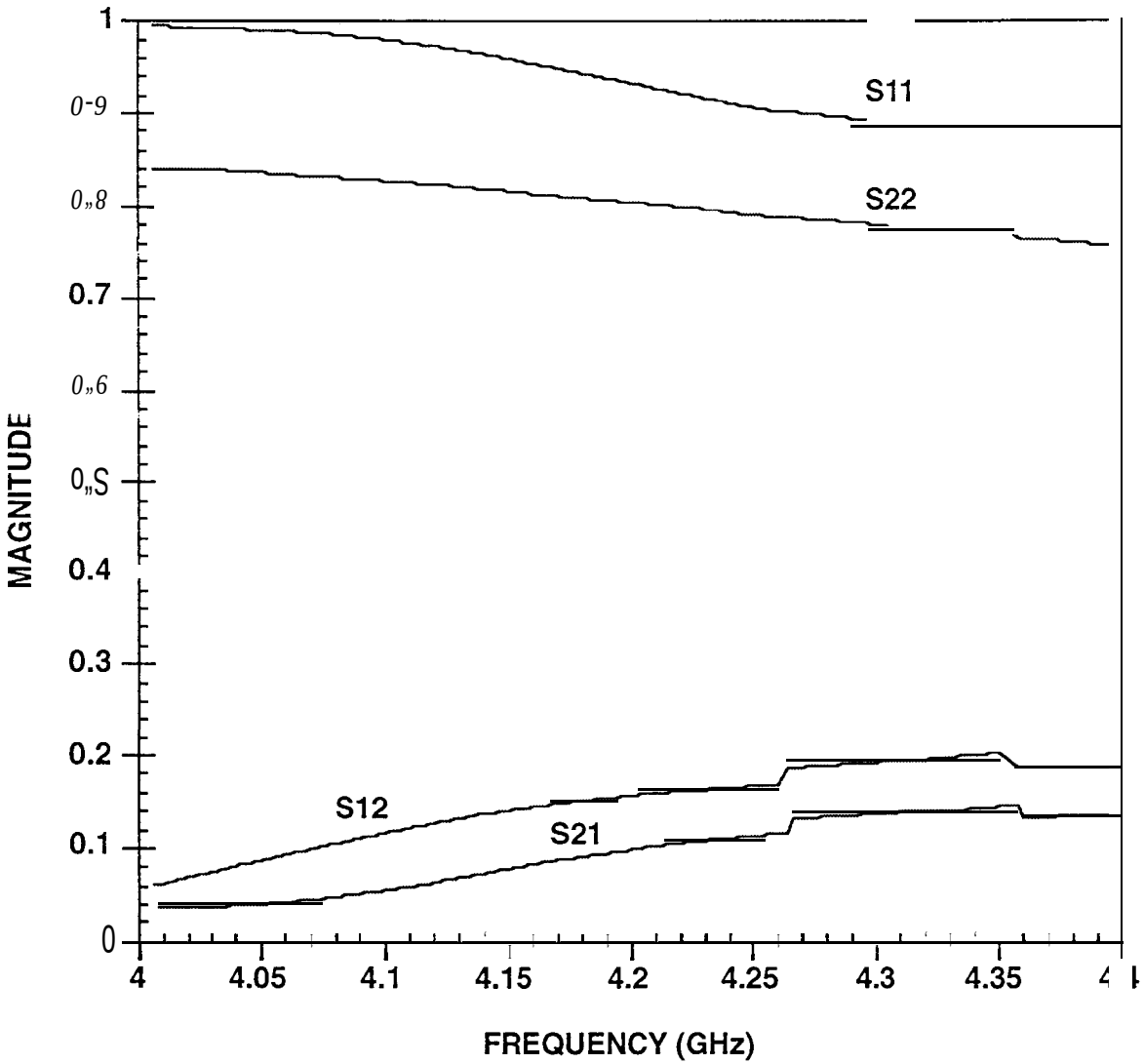

Fig. 12. Magnitude of de-embedded device S parameters, normalized to 50 ohms, when the unit cell shown in Fig. 9 is loaded with a differential pair HEMT biased at 0V.